PRODUCTION ENGINEERING ARCHIVES 2025, 31(4), 474-480

PRODUCTION ENGINEERING ARCHIVES

ISSN 2353-5156 (print)
ISSN 2353-7779 (online)

Exist since 4th quarter 2013
Available online at https://pea-journal.eu

Improvement of the cantilever test geometry deflection measurement method to assess residual stresses in laser powder bed fusion

Istvan Hatos[1*]

[1] Department of Materials Science and Technology, Széchenyi István University, 9026 Győr, Egyetem tér 1, Hungary
*Correspondence: hatos@sze.hu

Article history
Received 13.04.2025
Accepted 29.10.2025
Available online 12.12.2025

Keywords
additive manufacturing,
powder bed fusion,
internal stresses,
cantilever,
deformation.

Abstract
Laser powder bed fusion (L-PBF) processes allow for the creation of advanced 3D parts that are difficult to achieve through conventional manufacturing. Defects such as part deformation are a critical issue in L-PBF and seriously affect the industrial adoption of metal additive manufacturing (AM) processes for critical applications. The research community has widely accepted the deformation measurement of known geometries, such as cantilevers or bridges, for the assessment of residual stresses. In this study, quantitative measurements are obtained using a 3D optical scanner on cantilevers with different geometries, in order to study the effect of bar thickness on deformation. Furthermore, this experimental study aims to investigate cantilever deflection measurement methods and compare the obtained deviation parameters. The findings reveal that, in case of cantilever specimens, flatness and curvature attributes measured on surface are more reliable than maximum vertical deflection. The part height plays a primordial role on the deflection, the distortion changes in inverse proportion to the cantilever's bar thickness.

DOI: 10.30657/pea.2025.31.44

1. Introduction

Laser powder bed fusion (L-PBF) is one of the most widely used metal additive manufacturing (AM) technologies due to its ability to create advanced 3D parts that are difficult to achieve through conventional manufacturing (Bernard et al., 2023), along with their excellent mechanical properties (Zhang et al., 2023). Considering these advantages, it has a great future in various industries such as defense (Szachogłuchowicz et al., 2021), tooling (Zink et al., 2019), vehicle (Orosz et al., 2023; Erőss and Markovits, 2024), and biomedical (Kulcsar & Zsoldos, 2024; Lendvai et al., 2025). In L-PBF, thin layers of powder are spread by a recoater arm in a chamber with a controlled atmosphere and a high-energy laser beam is used to fully melt the thin layer of powder. After the solidification of one melted layer, the build plate lowers and a new layer of powder is spread by the recoater to be melted onto the previously solidified layer; this process continues until the part is complete. However, one of the main drawbacks of L-PBF is that it produces extremely high temperature gradients, caused by the high-energy laser beam and fast cooling rates during the solidification of the layers, which can lead to high stresses in the part. These large residual stresses may lead to distortion, component delamination, deformation, or even cracking during the L-PBF process (Chen et al., 2020; Levkulich et al., 2019).

Research on the deformation of components fabricated using L-PBF has attracted more attention in recent years. Many surveys have assessed the influences of process parameters on internal stresses (Levkulich et al., 2019; Mugwagwa et al., 2019; Mohammadtaheri et al., 2022; Zou et al., 2022) and it has been generally concluded that process variables have an important impact on the resulting residual stresses and part deformation, where decreasing the input energy can decrease internal stresses. Proper process conditions lead to a decrease in the temperature gradient; for example, pre-heating of the base plate (Ali et al., 2017), increasing the layer thickness (Zaeh & Branner, 2010), or the use of short scan vectors (Li et al.,

2018) can reduce the level of residual stresses. Residual stresses can also be reduced through heat treatment (Hatos et al., 2017; Edin et al., 2022).

There are two main directions for the analysis of residual stresses in AM components: quantifying the deformation caused by the stresses in manufactured geometries or evaluating the stresses within the material. Several characterization techniques have been used to measure residual stresses (e.g., hole drilling, contour, X-ray diffraction, and neutron diffraction), which generally generate quantitative data reflecting the stress state of the material. However, many of these techniques are costly or time-consuming, hindering their application at the industrial level (Edin et al., 2022; Robinson et al., 2018).

In deformation-based experiments, residual stress analysis requires the use of a known specific geometry. During full or partial separation from the substrate, the residual stresses are released and converted into deformation, and the deflection is measured. These deformation-based residual stress analysis methods utilize the inverse relationship between residual stresses and deformation. These methods are applicable for comparing the level of stress in the parts, as well as for calculation of the stresses that would have caused the measured deflections; however, they do not allow for the determination of the stress field of the part (Edin et al., 2022; Robinson et al., 2018). L-PBF processes create complex distributions of stress fields, such that the residual stresses in parts can be highly anisotropic and their magnitude can vary significantly (Xie et al., 2022; Acevedo et al., 2020; Zhang et al., 2023).

The distortion-based curvature method has been widely accepted by the research community, due to its sensitivity, simplicity, non-destructive nature, and applicability to various materials (Paraschiv et al., 2024). Cantilevers are structures directly printed on the built platform featuring long overhanging surfaces supported by thin, usually equally spaced supporting blocks and a solid block. The overhang beam can easily be distorted due to the residual stresses associated with the L-PBF process, distortion of the cantilevers occurs after the removal of the support structures from the substrate (Pauzon et al., 2021). Several studies have been performed on overhang cantilever test geometries, in order to investigate the influence of process parameters or to validate distortion prediction models. In literature works related to the experimental assessment of residual stresses connected with distortion, the authors have mainly considered 2D approaches. These methods consist of determining the difference between the maximum height of the specimen arms before and after separation from the support structure (Martucci et al., 2023; Mugwagwa et al., 2018; Meier et al., 2022; Jin et al., 2022), or on points along the longitudinal axis of the specimen (Noll et al., 2022). The measured deformation can then be input into finite element or analytical models to estimate the original stress state (Alzyod & Ficzere, 2022; Hanzl et al., 2020). The flatness deviation parameter and curvature attributes measured on 3D surface topographies are much more robust and repeatable than the distortion magnitude measured on isolated points. Compared to the 2D measurements generally reported in the literature, 3D characterization provides more relevant information with higher precision (Salem et al., 2020; Le Roux et al., 2018).

In the published literature, the effects of specimen height on residual stresses and deformation have not been well-examined and analyzed. Five cantilever samples were built with varying bar thicknesses (0.5, 1, 2, 3, and 5 mm) using AlSi10Mg powder (Buchbinder et al., 2013). The authors concluded that the distortion is dependent upon the bar thickness, with the largest distortion on the test geometry observed for the smallest bar thickness. In another study, cantilevers with three different thicknesses were used in both experiments and simulations. The maximum deformations of the as-built specimens with thicknesses of 1, 2.5, and 5 mm were 1.38, 0.68, and 0.41 mm, respectively, with the thicker cantilever being more resistant to deformation caused by residual stresses (Jin et al., 2022). Yu et al. (Yu et al., 2023) investigated the effect of heat treatment conditions on residual stress in 1.2709 steel. In their work, also cantilever-shaped specimens were used with various thicknesses (0.5, 1, 1.25, 2.5, and 5 mm) showing a complex distortion behavior. The specimens bent downward when the thickness was relatively thin (0.5 and 1 mm). The authors reported that the downward distortions of the thin cantilevers were due to the phase transformation of the maraging steel from martensite to austenite during the L-PBF. When the thickness was 1.25 mm, almost no deformation occurred, with further increase in the thickness, the deformation became upward.

In view of the above literature review, the measurement and analysis of residual stresses and the effect of part height on deformations have been less-examined, and contradictory findings regarding the influence of part height were shown in experiments This study investigates the effects of the part's dimensions on the deformation of the cantilever samples, considering the bar thickness. To observe and precisely determine the deformations, the residual stress distortion-based curvature method was used. The cantilever deflection measurement methods and deviation parameters are also assessed.

2. Experimental

2.1. Sample production

The test samples in this study were produced using an EOSINT M270 L-PBF machine (EOS GmbH – Krailling/Munich, Germany), equipped with a 200 W, 0.1 mm focus diameter ytterbium fiber laser. The material used for this experiment was 1.2709 (X3NiCoMoTi 18-9-5) gas-atomized powder with a chemical composition of 17-19% Ni, 8.5-9.5% Co, 4.5-5.2% Mo, 0.6-0.8% Ti, 0.05-0.15% Al, <0.5% Cr, <0.1% Mn, <0.1% Si, <0.03% C, and balanced Fe (all in wt.%). The following conditions were maintained constant during the experiment: 175 W laser power, 800 mm/s scan speed, 0.1 mm distance between tracks, 0.02 mm layer thickness, 10 mm stripe width, 0 mm stripe overlap, 40 °C building platform preheating, 67° scanning rotation between subsequent layers, and a stripe scanning strategy. The contouring, upskin, and down-skin parameters were deactivated. The relative density of the parts produced with this parameter set is higher than 99.8% (Hatos et al., 2024). Process parameters and scanning strategies can be varied to reduce the impact of residual stresses. However, laser power plays a more dominant role than other parameters. Optimizing these parameters involves trade-offs between build cost, time, and quality. Although scanning strategies such as island and chessboard reduce residual stresses, they add complexity to fabrication and reduce production efficiency (Kazemi Movahed *et al.*, 2025).

To assess part distortion, cantilever beams with different lengths, thicknesses, and heights were designed. Cantilevers with varying bar thicknesses (h = 1, 2, 3, 4, 5, 6, 8, 10, 12, 15, and 18 mm) were built, with their geometry shown in Fig. 1, in order to determine how their distortion depends upon the material thickness. In addition, six modified cantilevers with a bar thickness (h) of 13/23/33 mm and with and without a remaining solid block were also fabricated via L-PBF (Fig. 2). While the printed workpieces are fully detached, the standard cantilever-shaped specimens remain partially on the building platform. These samples were used to investigate the effect of partial and full cutting on the deflection. The red lines indicate the plane of the cut after printing. The size and number of test specimens were determined based on preliminary experiments, taking into account that they could be produced simultaneously without restarting the machine. Stopping and restarting the build process affects the thermal history of the parts, leading to changes in residual stress distributions (Mahtabi et al., 2023).

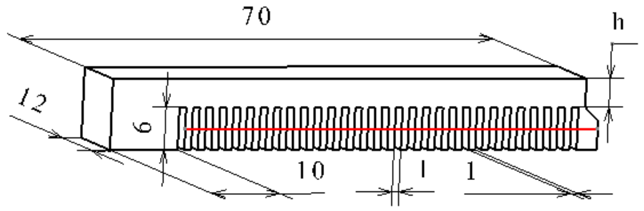

Fig. 1. A standard cantilever-shaped specimen with the cutting path

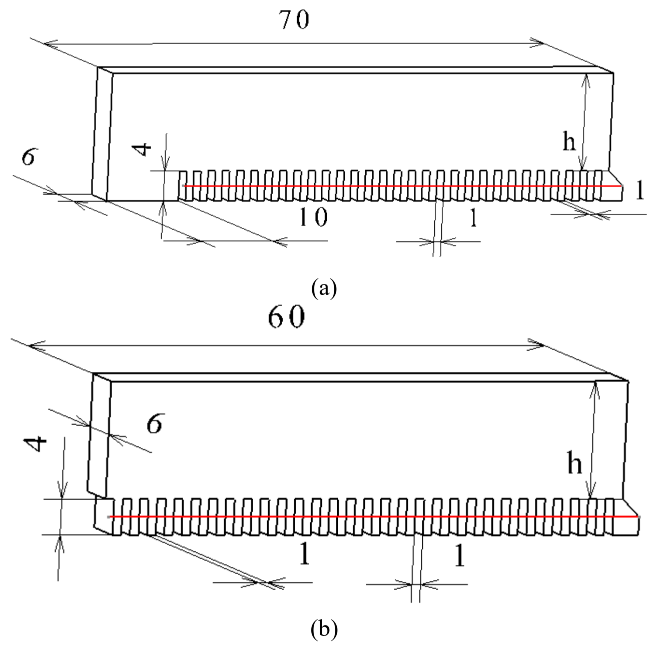

Fig. 2. Models of the modified cantilever-shaped specimens with the cutting path: (a) with a remaining solid block, and (b) without a remaining solid block

2.2. Distortion measurement

After production, the parts were partially cut from the base plate using wire electric discharge machining (WEDM). Contactless full-space measurements of the displacements and deformations of the specimens were performed using a digital optical measurement device. A blue-light 3D scanner (GOM ATOS Triple Scan – Braunschweig, Germany) was used to scan the surface of the fabricated specimens to obtain their 3D digital models. The accuracy of the 3D scanner system was ensured through compliance with ISO 10360 and VDI/VDE 2634 standards, supported by multi-step calibration procedures. The maximum permissible error of the system is limited to 0.01 mm. Then, the scanned geometries were compared with the designed models using GOM Inspect software, in order to obtain the dimension deviation of the cantilevers fabricated via L-PBF. During the evaluation process, a Gaussian best-fit algorithm based on the least squares method was used, in accordance with established metrological standards. This ensured that the calculated deviations reflected true geometric changes that were not influenced by surface roughness or measurement noise. The dimension deviation was used to evaluate the degree of distortion in the specimens considered in this work. The residual stresses could then be estimated by measuring the maximum deflection of the cantilever free-end after cutting the legs, as shown in Fig. 3. The maximum deflection measured serves as an indicator of the residual stresses present during the build, with a higher deflection result indicating higher stresses.

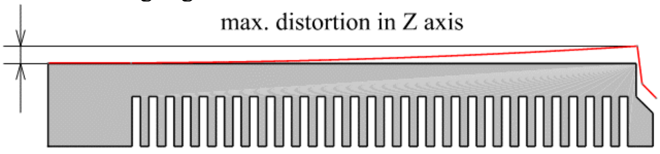

Fig. 3. Schematic visualization of the measurement of a cantilever's maximum deflection

The flatness deviation parameter has also been used in the literature (Salem et al., 2020; Le Roux et al., 2018) to compare the distortion caused by internal stresses. GOM Inspect software was used to measure flatness. Fig. 4 shows a representative image of the flatness measurement performed in the GOM Inspect software. The flatness parameter was determined at two areas: the entire upper surface including the solid block (FLTe) (Fig. 4a) and only the curved surface without the solid block (FLTc) above the cut legs (Fig. 4b).

In addition, the deformation was characterized according to the curvature attributes (K = 1/R), which is simply the reciprocal of the radius of curvature. Curvature describes how much the curve deviates from a straight line. The smaller the radius of curvature, the more bent the curve is and, hence, the larger the curvature (Roberts, 2001). The radius was determined on the centerline of the upper surface of the samples. The Gaussian best-fit method in GOM Inspect was used for radius fitting. Similar to the flatness deviation, Re (Ke) was determined on the centerline belonging to the entire upper surface with the solid block, while Rc (Kc) was determined on the centerline above the legs not including the solid block (Fig. 5).

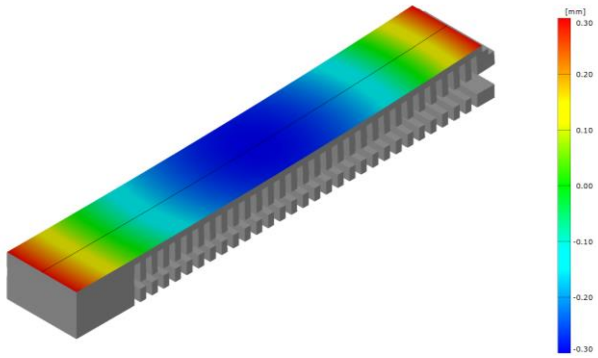

(a)

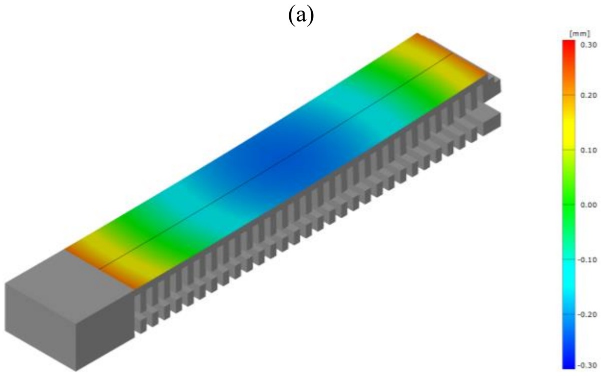

(b)

Fig. 4. Three-dimensional height maps showing the flatness deviation on (a) the entire upper surface (FLTe) with the centreline and on (b) the curved surface above the cut legs (FLTc) with the centerline

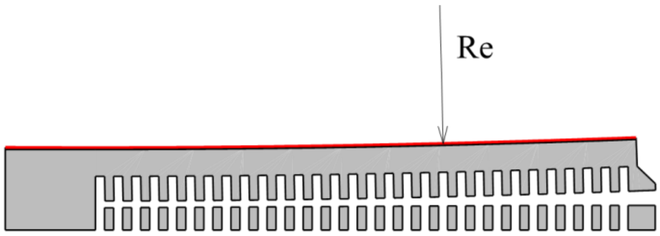

(a)

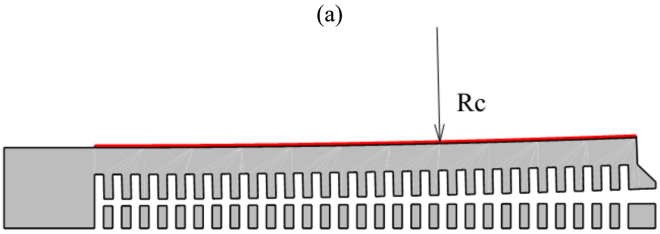

(b)

Fig. 5. Characterization of the curvature: (a) Re and (b) Rc

3. Results and discussion

In addition to the evaluation of residual stresses, a detailed analysis of the deformation affinity of the cantilevers was also carried out.

The cantilever specimens were built with different bar thicknesses. During manufacturing, in particular, the top layers of the specimens expanded due to the temperature increase caused by laser absorption. After cooling, a large tensile residual stress was induced in the top layers. It should be noted that no cracking or building failure was observed on the specimens. To allow for the release of residual stresses without the introduction of cutting forces, the centers of the support bars were cut using WEDM as a post-processing step. After the support structure between the cantilevers and the building platform was disjoined, the cantilever beam bent due to the release of the residual stresses (Fig. 6).

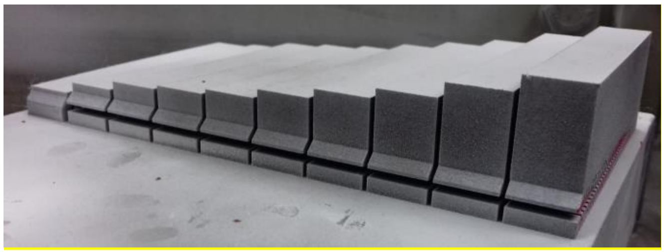

Fig. 6. Photograph of the wire-cut cantilever structures

Vertical displacement became the dominant deformation of the specimens. Generally, the cantilevers bent upward, except for the specimen with 1 mm bar thickness; this specimen was observed to bend downward (Fig. 7), in contrast to what is expected from the literature (Jin et al., 2022; Buchbinder et al., 2013), where the largest distortion on the test geometry was measured with the smallest bar thickness in case of 316L and AlSi10Mg powders. Cantilevers with different bar thicknesses manufactured from 1.2709 maraging steel were studied by Yu et al. (Yu et al., 2023), who found a similar complex distortion behaviour: the cantilever-shaped specimens bent downward significantly when the thicknesses were relatively thin (0.5 and 1 mm). According to these researchers, the downward distortions of the thin cantilevers were due to the phase transformation of the maraging steel from martensite to austenite. Further experiments are required to verify the observed phenomenon.

Fig. 7. Photograph of the specimen with 1 mm bar thickness

The downward displacement observed for the specimen with 1 mm bar thickness exceeded the thickness of the WEDM cutting gap, so the maximum downward displacement could not be measured. The results measured for this specimen are therefore not displayed in this article.

The overall deformation of all the samples was measured using a GOM optical scanner. A comparison was made using the height (Z value) references of the edges at the end of each beam. Flatness deviations (FLTe and FLTc) and curvature attributes (Ke and Kc) were determined from the scanned samples in GOM Inspect software.

Fig. 8 depicts the measured Z-direction displacement distribution with different bar thicknesses. The displacement distributions of all the cantilever samples are similar, but the deformation level decreases with bar thickness.

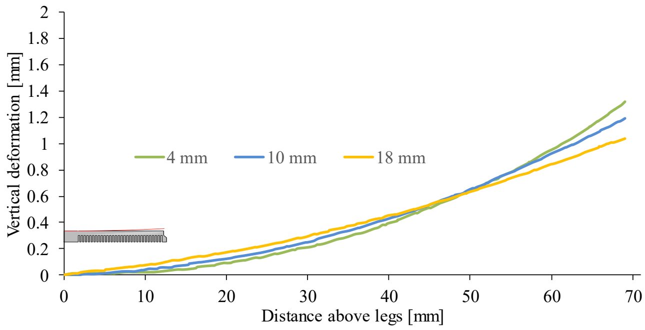

Fig. 8. Deformation of cantilevers along the top surface centerline, depending on bar thickness (4, 10, and 18 mm)

The relationship between the maximum deflection of the cantilevers and bar thickness is shown in Fig. 9. Based on the results, when the thickness of the cantilevers increases, the deformation measured at the end of the beams decreases. In the case of low bar thickness, the relationship with deflection is less clear. Meanwhile, when the bar thickness is above 6 mm, the results show a good linear relationship.

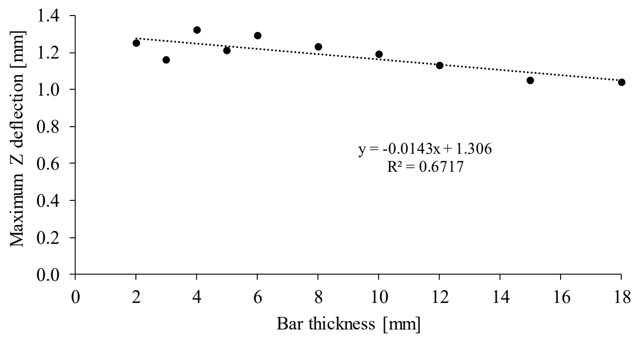

Fig. 9. Maximum Z deflection as a function of bar thickness

The experimental measurements of flatness distortion based on the 3D scanner data are compiled in Fig. 10.

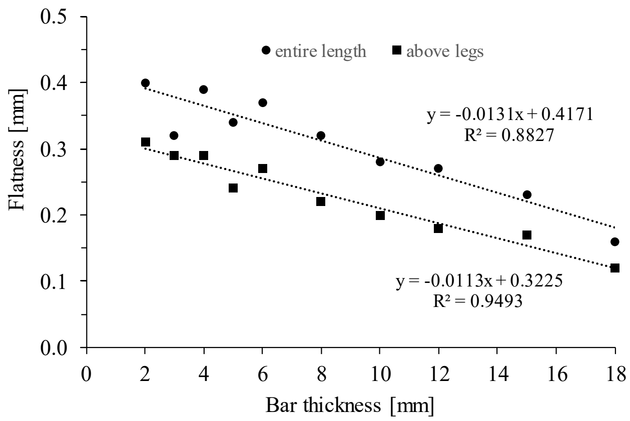

Fig. 10. Evolution of the flatness deviation of specimens with different bar thicknesses

A concave-shaped distortion formed on the test specimens. The gradient of plastic deformation (strain) mainly dominated in the building direction (Z) (Buchbinder et al., 2013), and the distortion in the part transverse direction was negligible. As expected, the flatness distortion measured on a smaller area (above the legs) showed a smaller deviation than that measured on a larger area. A linear relationship was observed between the thickness of the part and the flatness measurement; this is due to the greater stiffness of bars with greater thickness.

The radius was determined on the centerline of the upper surface of the samples, and the Gaussian best-fit method in GOM Inspect was used for radius fitting. Similar to the flatness deviation, Re (Ke) was determined on the centerline of the entire upper surface, while Rc (Kc) was determined on the centerline above the legs.

The curvature measurement-based evaluation also showed a similar trend to the previous tests. A strong linear relationship was found between bar thickness and the inverse of the fitted radius (Fig. 11). The coefficient of determination (R^2) values of the linear correlations were 0.96 for Kc and 0.97 for Ke. The values measured on the centerlines of the full length and above the legs were very close, and this measurement method was considered to be less sensitive to the measurement length.

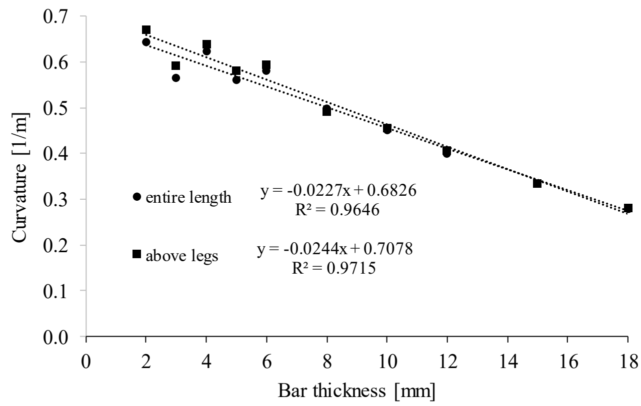

Fig. 11. Plot of curvature as a function of bar thickness

All three evaluations showed a linear decreasing trend; therefore, it can be stated that the deformation decreases with increasing thickness and, after reaching a certain thickness, the workpiece/test specimen is assumed to not deform. In this case, the workpiece will still not be free of internal stress; however, its stiffness is greater than the internal stress that builds up. The prediction based on the radius and flatness measurements indicates freedom from deformation at around 30 mm thickness. The slope of the line fitted to the maximum Z deformation was much smaller than those of the lines fitted to the points of the other two measurements. This led to a marked difference in the prediction, indicating freedom from deformation at 100 mm.

A real AM part is completely removed from the base plate, while during the experiment, only the ribbed half of the cantilever specimens was cut off. The samples were designed (Fig. 2b) and manufactured with or without a remaining solid block to investigate the effect of full and partial cutting on the previously applied deformation metrics. The overall deformation of all the modified samples was also measured using a GOM optical scanner. Flatness deviations (FLTc) and curvature attributes (Kc) were determined on fully and partially cut specimens. Nearly the same flatness and curvature metrics were measured for cantilevers with equal thicknesses. The remaining solid block had no significant effect on deformation.

4. Conclusions

To observe and precisely determine the deformations resulting from the L-PBF process, the residual stress distortion-based curvature method was used. For this purpose, cantilevers with varying bar thicknesses were built. The overall deformation of all the samples was measured using a GOM optical scanner. Based on the improvement in determining the distortion of cantilever specimens after separation, criteria such as the maximum Z deflection, flatness deviations (FLTe and FLTc), and curvature attributes (Ke and Kc) were determined from 3D measurements of the upper surface. The following conclusions could be drawn:

- The L-PBF parts printed from different base materials showed significant differences in the magnitude and direction of distortion in the case of low part thicknesses.
- In the as-built state, the L-PBF 1.2709 steel cantilevers showed complex deformation behaviour after the support structure between the cantilevers and the building platform was cut. The specimen bent downward when the thickness was relatively thin (1 mm) and bent upward when the thickness was at least 2 mm.
- The deformation of the specimens decreased with increasing thickness; note that this statement is based on the measurement results of specimens with a thickness of at least 2 mm.
- Based on the results, it can be stated that there is a relationship between the deformation of metal 3D-printed specimens and the height of the specimen; in the case of the material and technology examined in this study, this relationship is linear.
- In the case of cantilever specimens, instead of the maximum deflection, the flatness measurement and curvature are more reliable, providing values that present the same tendency as the deformation of the fully cut specimen.
- The slopes of the lines fitted to the flatness and curvature results are nearly identical, while the slope of the line fitted to the maximum vertical deformation data is smaller.
- The lines fitted to the deformation data can be used to predict the thickness at which a specimen is free of deformation.
- Flatness and curvature better reflect the real deformation phenomenon, compared to the maximum vertical deformation.

Acknowledgements

Project no. TKP2021-NVA-23 has been implemented with the support provided by the Ministry of Innovation and Technology of Hungary from the National Research, Development and Innovation Fund, financed under the TKP2021-NVA funding scheme.

References

Acevedo, R., Sedlak, P., Kolman, R., Fredel, M. 2020. Residual stress analysis of additive manufacturing of metallic parts using ultrasonic waves: State of the art review. Journal of Materials Research and Technology, 9(4), 9457-9477. DOI: 10.1016/j.jmrt.2020.05.092

Ali, H., Ma, L., Ghadbeigi, H., Mumtaz, K. 2017. In-situ residual stress reduction, martensitic decomposition and mechanical properties enhancement through high temperature powder bed pre-heating of Selective Laser Melted Ti6Al4V. Materials Science and Engineering: A, 695, 211-220. DOI: 10.1016/j.msea.2017.04.033

Alzyod, H., Ficzere, P. 2022. Finite Element Modeling of Additive Manufacturing in Case of Metal Parts. Periodica Polytechnica Transportation Engineering, 50(4), 330-335. DOI: 10.3311/PPtr.19242

Bernard, A., Kruth, J.-P., Cao, J., Lanza, G., Bruschi, S., Merklein, M., Vaneker, T., et al. 2023. Vision on metal additive manufacturing: Developments, challenges and future trends. CIRP Journal of Manufacturing Science and Technology, 47, 18-58. DOI: 10.1016/j.cirpj.2023.08.005

Buchbinder, D., Meiners, W., Pirch, N., Wissenbach, K., Schrage, J. 2013. Investigation on reducing distortion by preheating during manufacture of aluminum components using selective laser melting. Journal of Laser Applications, 26(1), 012004. DOI: 10.2351/1.4828755

Chen, C., Chang, S., Zhu, J., Xiao, Z., Zhu, H., Zeng, X. 2020. Residual stress of typical parts in laser powder bed fusion. Journal of Manufacturing Processes, 59, 621-628. DOI: 10.1016/j.jmapro.2020.10.009

Edin, E., Svahn, F., Åkerfeldt, P., Eriksson, M., Antti, M.-L. 2022. Rapid method for comparative studies on stress relief heat treatment of additively manufactured 316L. Materials Science and Engineering: A, 847, 143313. DOI: 10.1016/j.msea.2022.143313

Erőss, L.D., Markovits, T. 2024. Mass reduction method for topology optimisation of a Ti6Al4V part for additive manufacturing. Production Engineering Archives, 30(3), 354-360. DOI: 10.30657/pea.2024.30.35

Hanzl, P., Zetková, I., Daňa, M., Nozar, M. 2020. Advanced Simulation of Metal Additive Manufacturing Using Maraging Steel and Nickel Alloy. Manufacturing Technology, 20(3), 313-317. DOI: 10.21062/mft.2020.045

Hatos, I., Hargitai, H., Kovács, J.G. 2017. Characterization of Internal Stresses in Hybrid Steel Structures Produced by Direct Metal Laser Sintering. Materials Science Forum, 885, 196-201. DOI: 10.4028/www.scientific.net/MSF.885.196

Hatos, I., Hargitai, H., Fekete, G., Fekete, I. 2024. Effect of Energy Density on the Mechanical Properties of 1.2709 Maraging Steel Produced by Laser Powder Bed Fusion. Materials, 17(14), 3432. DOI: 10.3390/ma17143432

Jin, Q.-Y., Kang, D., Ha, K., Yu, J.H., Lee, W. 2022. Simulation of annealing process on AISI 316 L stainless steel fabricated via laser powder bed fusion using finite element method with creep. Additive Manufacturing, 60, 103255. DOI: 10.1016/j.addma.2022.103255

Kazemi Movahed, A., Ghanavati, R., Saboori, A., Iuliano, L. 2025. A Review of Strategies for In Situ Mitigating of Residual Stress in Laser-Based Metal Additive Manufacturing: Insights, Innovations, and Challenges. Acta Metallurgica Sinica (English Letters), 38(10), 1657-1698. DOI: 10.1007/s40195-025-01902-5

Kulcsar, K., Zsoldos, I. 2024. Mechanical Studies of Subperiosteal Implants. Periodica Polytechnica Mechanical Engineering, 68(1), 53-62. DOI: 10.3311/PPme.23706

Le Roux, S., Salem, M., Hor, A. 2018. Improvement of the bridge curvature method to assess residual stresses in selective laser melting. Additive Manufacturing, 22, 320-329. DOI: 10.1016/j.addma.2018.05.025

Lendvai, L., Fekete, I., Rigotti, D., Pegoretti, A. 2025. Experimental study on the effect of filament-extrusion rate on the structural, mechanical and thermal properties of material extrusion 3D-printed polylactic acid (PLA) products. Progress in Additive Manufacturing, 10(1), 619-629. DOI: 10.1007/s40964-024-00646-5

Levkulich, N.C., Semiatin, S.L., Gockel, J.E., Middendorf, J.R., DeWald, A.T., Klingbeil, N.W. 2019. The effect of process parameters on residual stress evolution and distortion in the laser powder bed fusion of Ti-6Al-4V. Additive Manufacturing, 28, 475-484. DOI: 10.1016/j.addma.2019.05.015

Li, Z., Xu, R., Zhang, Z., Kucukkoc, I. 2018. The influence of scan length on fabricating thin-walled components in selective laser melting. International Journal of Machine Tools and Manufacture, 126, 1-12. DOI: 10.1016/j.ijmachtools.2017.11.012

Mahtabi, M., Yadollahi, A., Stokes, R., Doude, H., Priddy, M. 2023. Effect of build interruption during laser powder bed fusion process on structural integrity of Ti-6Al-4V. Engineering Failure Analysis, 153, 107626. DOI: 10.1016/j.engfailanal.2023.107626

Martucci, A., Marchese, G., Bassini, E., Lombardi, M. 2023. Effects of Stress-Relieving Temperature on Residual Stresses, Microstructure and Mechanical Behaviour of Inconel 625 Processed by PBF-LB/M. Metals, 13(4), 796. DOI: 10.3390/met13040796

Meier, B., Godja, N., Warchomicka, F., Belei, C., Schäfer, S., Schindel, A., Palcynski, G., et al. 2022. Influences of Surface, Heat Treatment, and Print Orientation on the Anisotropy of the Mechanical Properties and the Impact Strength of Ti 6Al 4V Processed by Laser Powder Bed Fusion. Journal of Manufacturing and Materials Processing, 6(4), 87. DOI: 10.3390/jmmp6040087

Mohammadtaheri, H., Sedaghati, R., Molavi-Zarandi, M. 2022. Inherent strain approach to estimate residual stress and deformation in the laser powder bed fusion process for metal additive manufacturing—a state-of-the-art review. The International Journal of Advanced Manufacturing Technology, 122(5-6), 2187-2202. DOI: 10.1007/s00170-022-10052-2

Mugwagwa, L., Dimitrov, D., Matope, S., Yadroitsev, I. 2018. Influence of process parameters on residual stress related distortions in selective laser melting. Procedia Manufacturing, 21, 92-99. DOI: 10.1016/j.promfg.2018.02.099

Mugwagwa, L., Yadroitsev, I., Matope, S. 2019. Effect of Process Parameters on Residual Stresses, Distortions, and Porosity in Selective Laser Melting of Maraging Steel 300. Metals, 9(10), 1042. DOI: 10.3390/met9101042

Noll, I., Koppka, L., Bartel, T., Menzel, A. 2022. A micromechanically motivated multiscale approach for residual distortion in laser powder bed fusion processes. Additive Manufacturing, 60, 103277. DOI: 10.1016/j.addma.2022.103277

Orosz, T., Horváth, T., Tóth, B., Kuczmann, M., Kocsis, B. 2023. Iron Loss Calculation Methods for Numerical Analysis of 3D-Printed Rotating Machines: A Review. Energies, 16(18), 6547. DOI: 10.3390/en16186547

Paraschiv, A., Matache, G., Vladut, M. 2024. Assessment of Residual Stresses in Laser Powder Bed Fusion Manufactured IN 625. Materials, 17(2), 413. DOI: 10.3390/ma17020413

Pauzon, C., Mishurova, T., Evsevleev, S., Dubiez-Le Goff, S., Murugesan, S., Bruno, G., Hryha, E. 2021. Residual stresses and porosity in Ti-6Al-4V produced by laser powder bed fusion as a function of process atmosphere and component design. Additive Manufacturing, 47, 102340. DOI: 10.1016/j.addma.2021.102340

Roberts, A. 2001. Curvature attributes and their application to 3D interpreted horizons. First Break, 19(2), 85-100. DOI: 10.1046/j.0263-5046.2001.00142.x

Robinson, J., Ashton, I., Fox, P., Jones, E., Sutcliffe, C. 2018. Determination of the effect of scan strategy on residual stress in laser powder bed fusion additive manufacturing. Additive Manufacturing, 23, 13-24. DOI: 10.1016/j.addma.2018.07.001

Salem, M., Le Roux, S., Hor, A., Dour, G. 2020. A new insight on the analysis of residual stresses related distortions in selective laser melting of Ti-6Al-4V using the improved bridge curvature method. Additive Manufacturing, 36, 101586. DOI: 10.1016/j.addma.2020.101586

Szachogłuchowicz, I., Fikus, B., Grzelak, K., Kluczyński, J., Torzewski, J., Łuszczek, J. 2021. Selective Laser Melted M300 Maraging Steel—Material Behaviour during Ballistic Testing. Materials, 14(10), 2681. DOI: 10.3390/ma14102681

Xie, D., Lv, F., Yang, Y., Shen, L., Tian, Z., Shuai, C., Chen, B., et al. 2022. A Review on Distortion and Residual Stress in Additive Manufacturing. Chinese Journal of Mechanical Engineering: Additive Manufacturing Frontiers, 1(3), 100039. DOI: 10.1016/j.cjmeam.2022.100039

Yu, J.H., Jin, Q.-Y., Ha, K., Lee, W. 2023. Influence of Several Heat Treatments on Residual Stress in Laser Powder Bed-Fused Maraging 18Ni-300 Steel. Applied Sciences, 13(11), 6572. DOI: 10.3390/app13116572

Zaeh, M.F., Branner, G. 2010. Investigations on residual stresses and deformations in selective laser melting. Production Engineering, 4(1), 35-45. DOI: 10.1007/s11740-009-0192-y

Zhang, Y., Lin, W., Zhai, Z., Wu, Y., Yang, R., Zhang, Z. 2023. Enhancing the mechanical property of laser powder bed fusion CoCrMo alloy by tailoring the microstructure and phase constituent. Materials Science and Engineering: A, 862, 144449. DOI: 10.1016/j.msea.2022.144449

Zink, B., Kovács, N.K., Kovács, J.G. 2019. Thermal analysis based method development for novel rapid tooling applications. International Communications in Heat and Mass Transfer, 108, 104297. DOI: 10.1016/j.icheatmasstransfer.2019.104297

Zou, S., Pang, L., Xu, C., Xiao, X. 2022. Effect of Process Parameters on Distortions Based on the Quantitative Model in the SLM Process. Applied Sciences, 12(3), 1567. DOI: 10.3390/app12031567